Electronic Supplementary Information

Just add water to split water: ultra-high-performance bifunctional electrocatalyst by eco-friendly heterointerfacing Ni-Co diselenides

Dongliang Chen,[a] Zhenmiao Xu,[a] Wei Chen,[b] Guangliang Chen,*[a] Jun Huang,*[b,c] Changsheng Song,*[a] Chaorong Li[a] and Kostya (Ken) Ostrikov[c,d]

[a]School of Materials Science and Engineering, Zhejiang Sci-Tech University, Hangzhou 310018, China

*E-mail: glchen@zstu.edu.cn; cssong@zstu.edu.cn

[b]School of Physics and Electronic Information, Gannan Normal University, Ganzhou, Jiangxi 341000, China

*E-mail: junhuang66@163.com

[c]School of Chemistry and Physics, Queensland University of Technology, Brisbane, QLD 4000, Australia

[d]Centre for Materials Science, Queensland University of Technology, Brisbane, QLD 4000, Australia

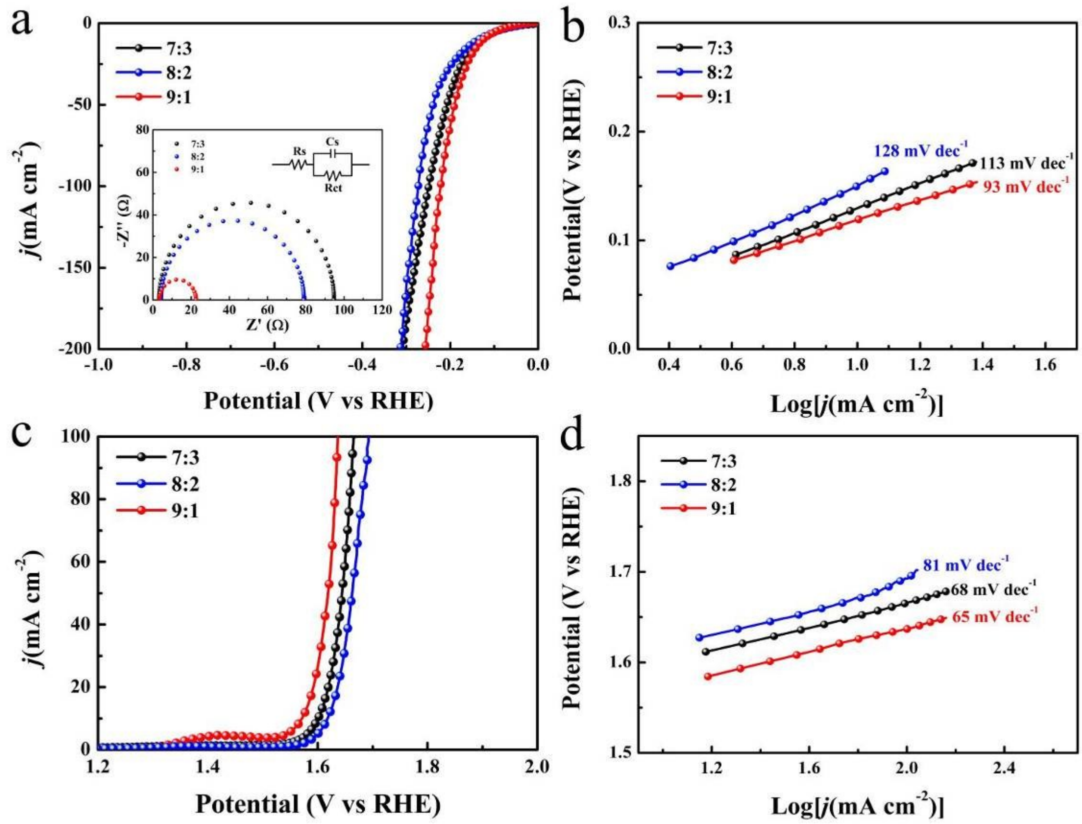

Figure S1. The effects of different Ni/Co alloy ratio on the HER and OER activity of the in-situ fabricated NiCo LDH/NCF. (a) Polarization curves in 1 M KOH for the HER with a scan rate of 1 mV s^{-1} and the insert is the corresponding Nyquist plots, (b) The Tafel plots corresponding to HER polarization curves, (c) Polarization curves in 1 M KOH for the OER with a scan rate of 1 mV s^{-1}, and (d) The Tafel plots corresponding to OER polarization curves.

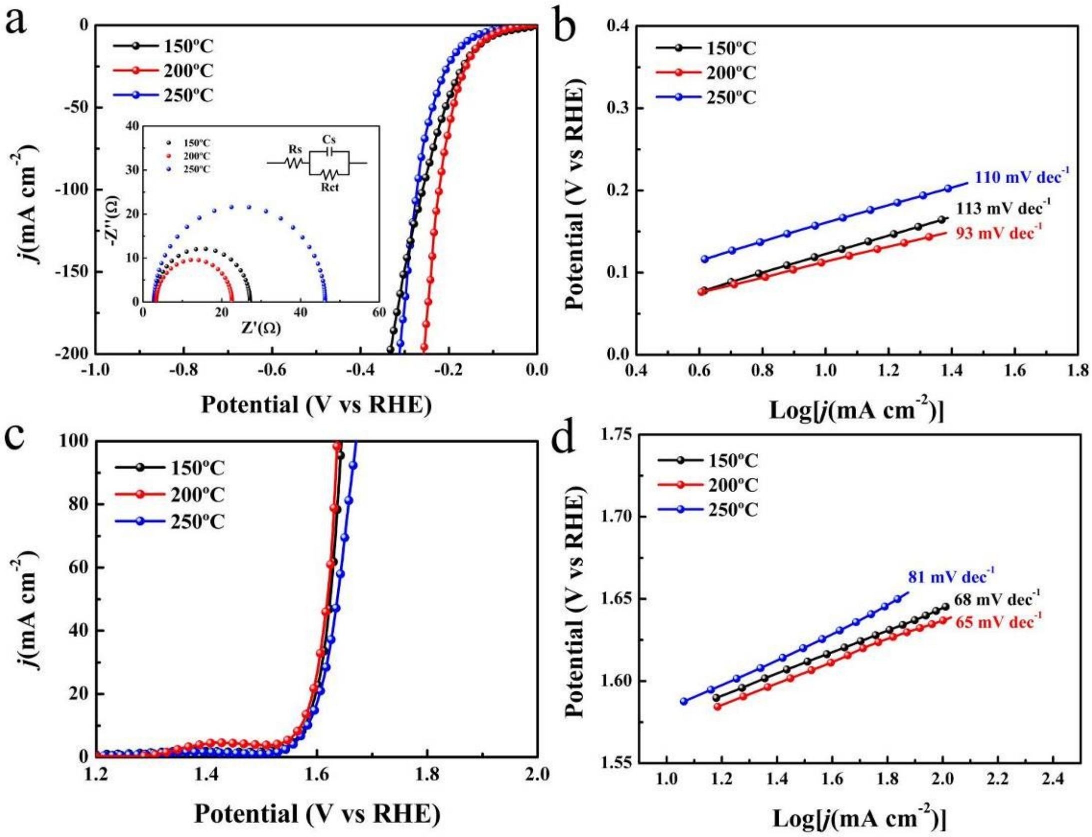

Figure S2. The HER and OER performances of in-situ NiCo LDH/NCF fabricated with different reaction temperature. (a) Polarization curves in 1 M KOH for the HER with a scan rate of 1 mV s^{-1}, and the insert is the corresponding Nyquist plots, (b) The Tafel plots corresponding to HER polarization curves, (c) Polarization curves in 1 M KOH for the OER with a scan rate of 1 mV s^{-1}, (d) The Tafel plots corresponding to OER polarization curves.

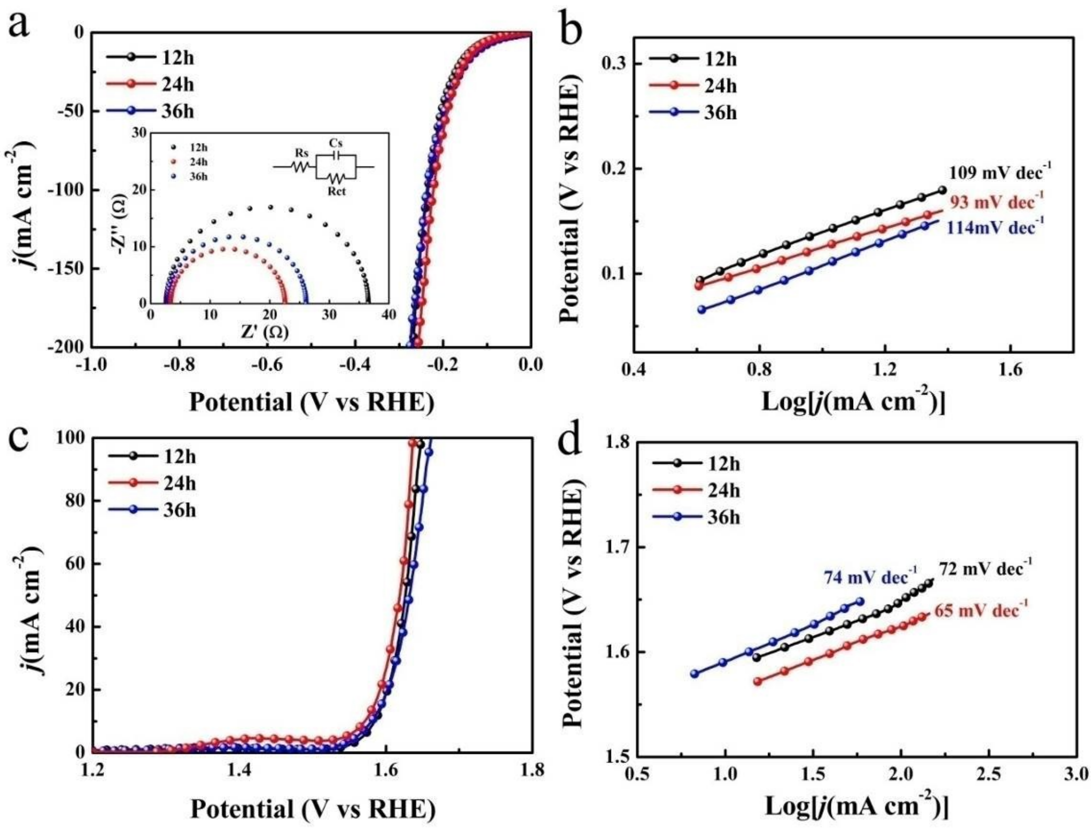

Figure S3. The HER and OER performances of in-situ NiCo LDH/NCF fabricated with different reaction time. (a) Polarization curves in 1 M KOH for the HER with a scan rate of 1 mV s^{-1} and the insert is the corresponding Nyquist plots, (b) The Tafel plots corresponding to HER polarization curves, (c) Polarization curves in 1 M KOH for the OER with a scan rate of 1 mV s^{-1} and (d) The Tafel plots corresponding to OER polarization curves.

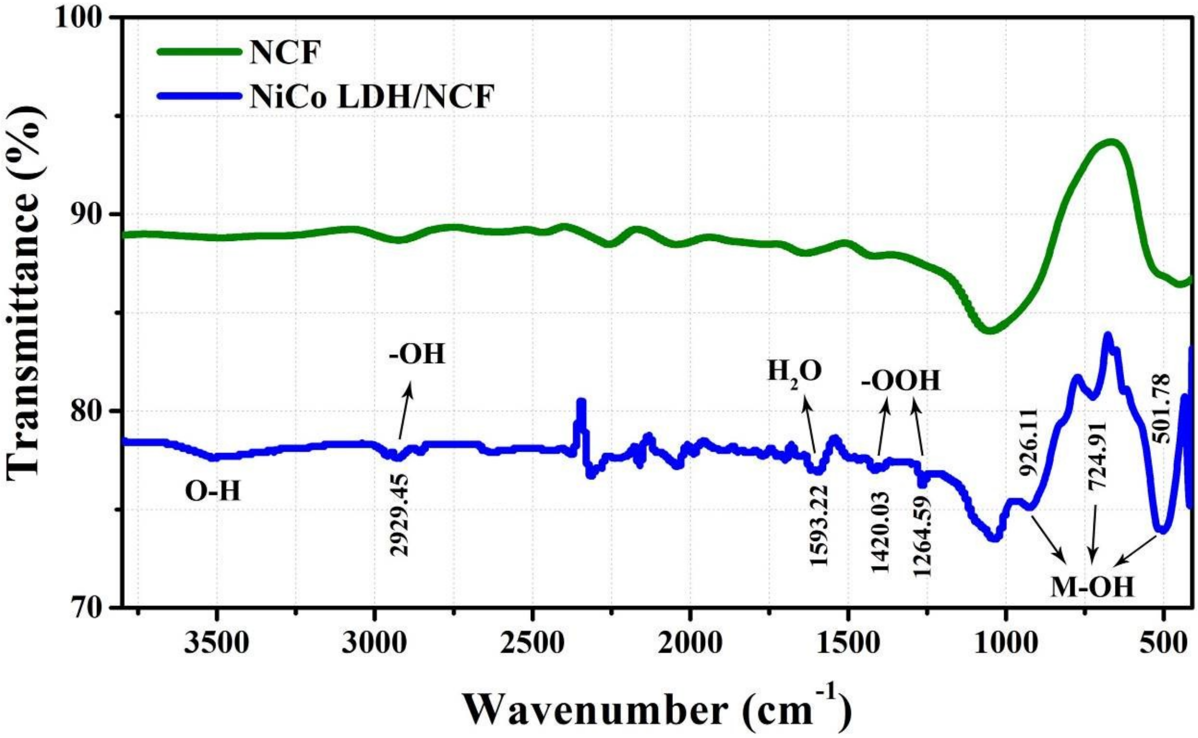

Figure S4. The FTIR spectrum of NiCo LDH sprouted from NCF surface.

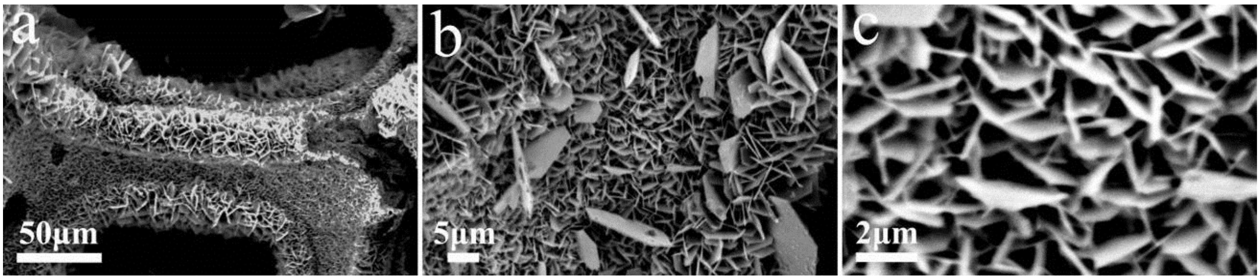

Figure S5. The SEM images of in-situ NiCo LDH/NCF fabricated with optimized reaction conditions. (a) and (b) Low resolution SEM image, and (c) High resolution SEM image.

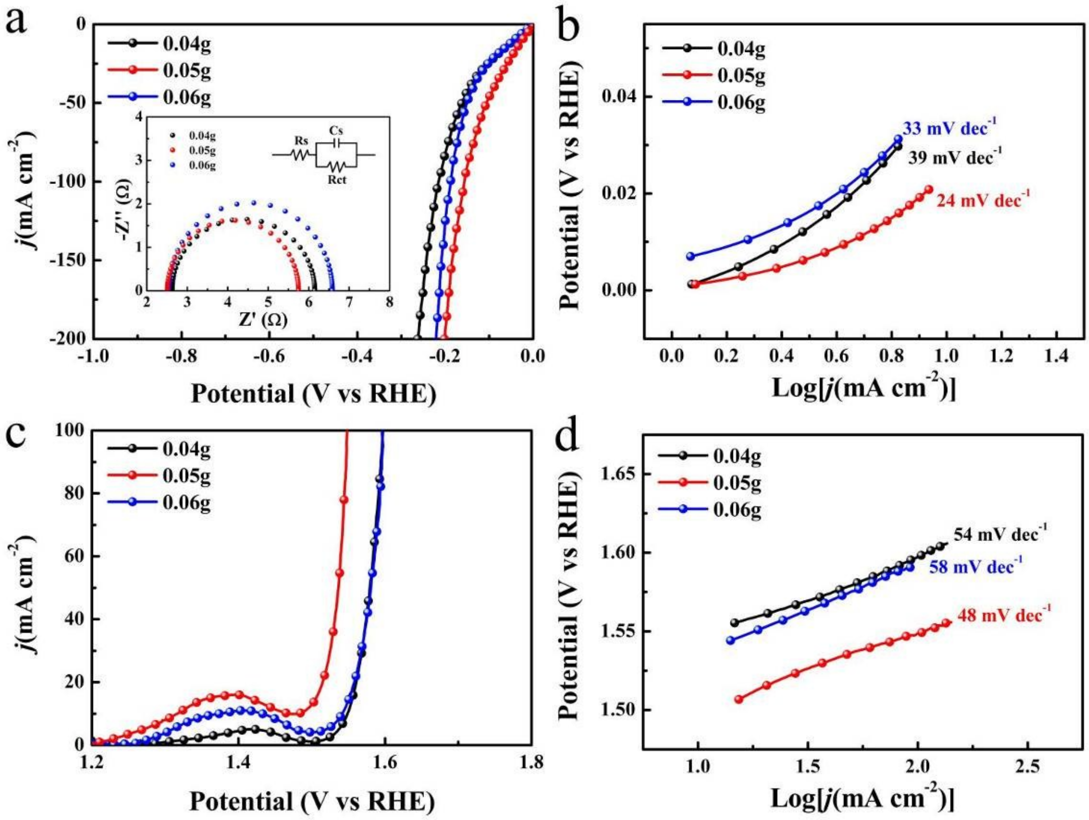

Figure S6. The effects of selenium powder amount on the HER and OER activity during selenization. (a) Polarization curves in 1 M KOH for the HER with a scan rate of 1 mV s^{-1} and the insert is the corresponding Nyquist plots, (b) The Tafel plots corresponding to HER polarization curves, (c) Polarization curves in 1 M KOH for the OER with a scan rate of 1 mV s^{-1} and (d) The Tafel plots corresponding to OER polarization curves.

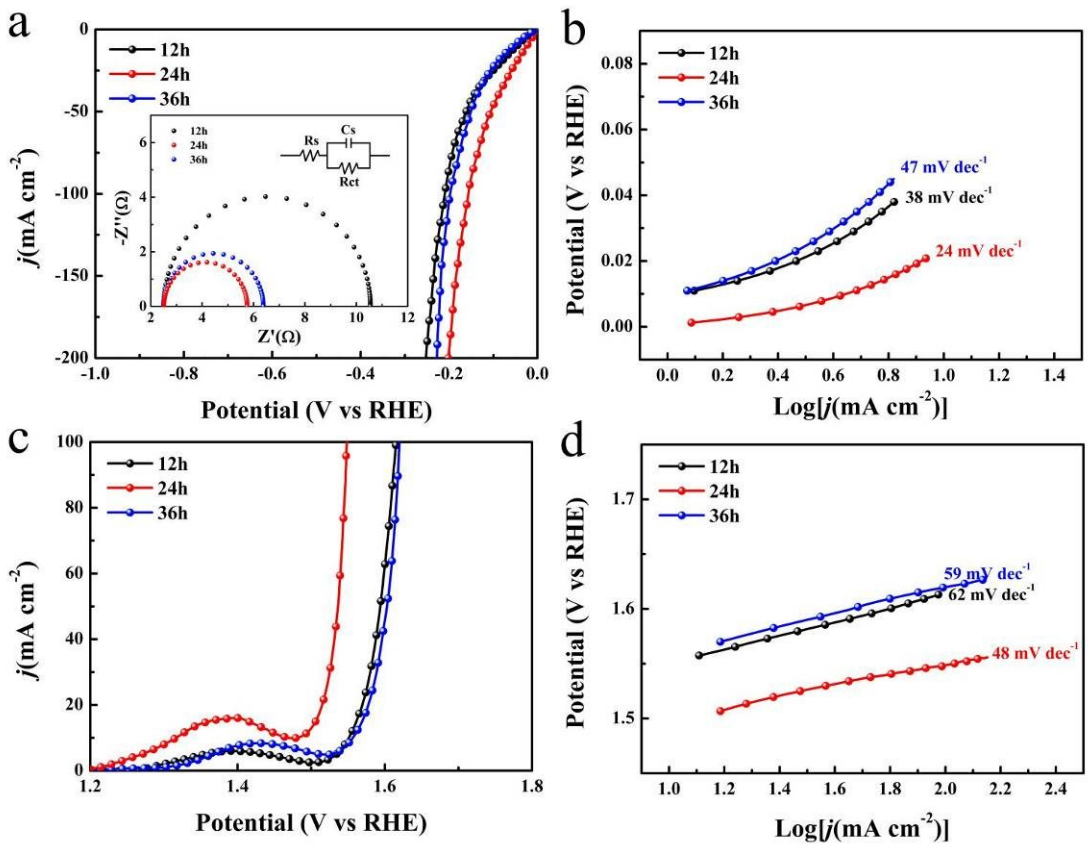

Figure S7. The HER and OER performances of $NiSe_2$-$CoSe_2$/NCF based on the in-situ NiCo LDH/NCF fabricated with different reaction time. (a) Polarization curves in 1 M KOH for the HER with a scan rate of 1 mV s^{-1} and the insert is the corresponding Nyquist plots, (b) The Tafel plots corresponding to HER polarization curves, (c) Polarization curves in 1 M KOH for the OER with a scan rate of 1 mV s^{-1} and (d) The Tafel plots corresponding to OER polarization curves.

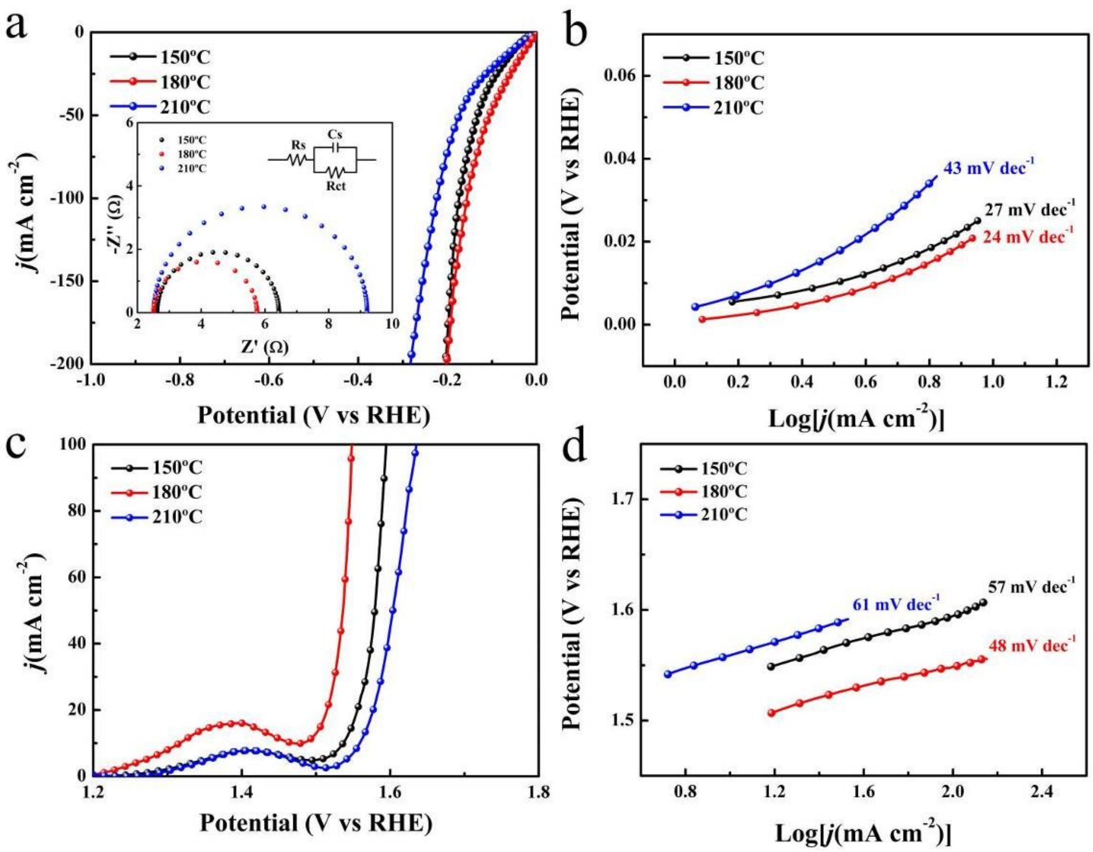

Figure S8. The HER and OER performances of $NiSe_2$-$CoSe_2$/NCF based on the in-situ NiCo LDH/NCF fabricated with different reaction temperature. (a) Polarization curves in 1 M KOH for the HER with a scan rate of 1 mV s^{-1} and the insert is the corresponding Nyquist plots, (b) The Tafel plots corresponding to HER polarization curves, (c) Polarization curves in 1 M KOH for the OER with a scan rate of 1 mV s^{-1} and (d) The Tafel plots corresponding to OER polarization curves.

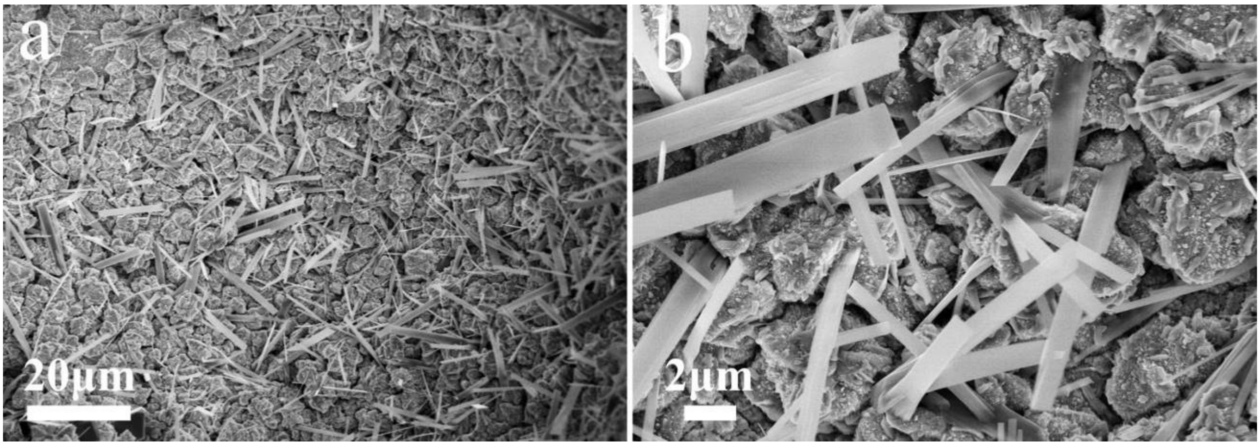

Figure S9. The SEM images of $NiCoSe_2$/NCF without the in-situ hydrothermal treatment. (a) Low resolution SEM image and (b) High resolution SEM image.

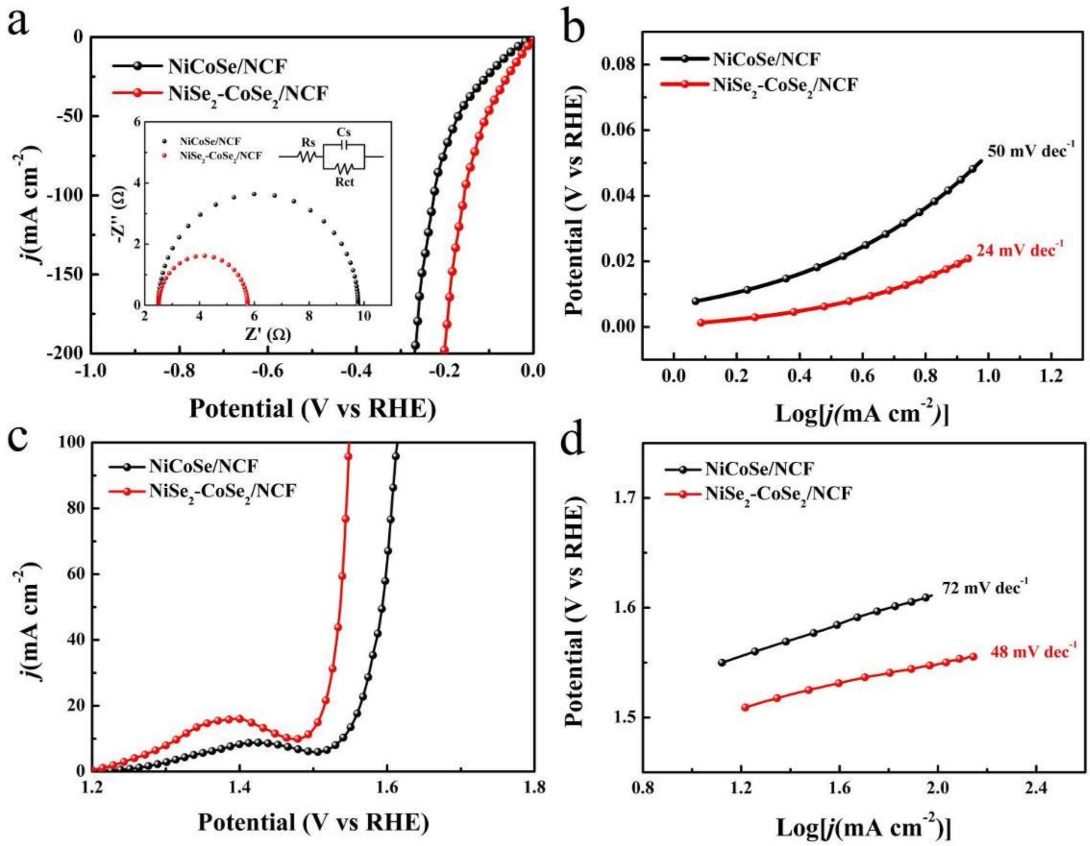

Figure S10. The effects of in-situ hydrothermal treatment on the HER and OER activity of the nickel-cobalt selenides. (a) Polarization curves in 1 M KOH for the HER with a scan rate of 1 mV s^{-1} and the insert is the corresponding Nyquist plots, (b) The Tafel plots corresponding to HER polarization curves, (c) Polarization curves in 1 M KOH for the OER with a scan rate of 1 mV s^{-1}, and (d) The Tafel plots corresponding to OER polarization curves.

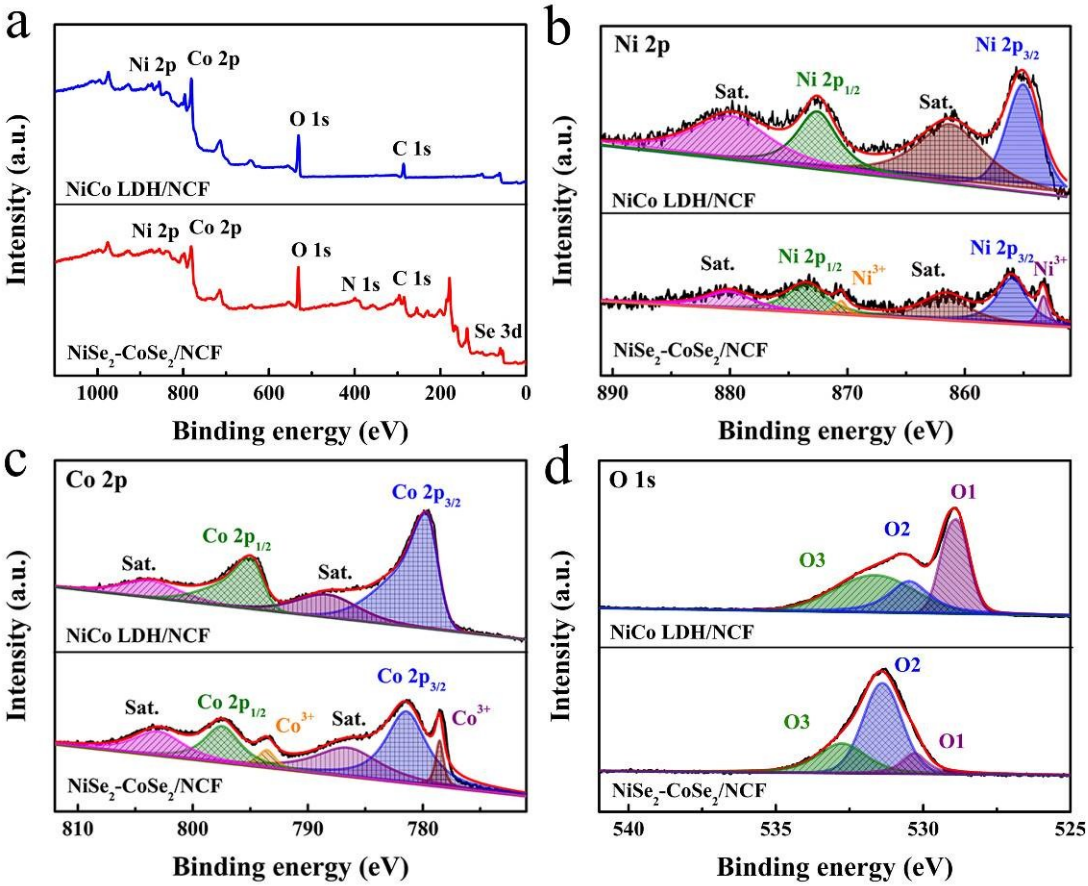

Figure S11. High resolution XPS spectra of NiCo LDH/NCF and $NiSe_2$-$CoSe_2$/NCF. (a) The whole spectra, (b) Ni 2p, (c) Co 2p, and (d) O 1s.

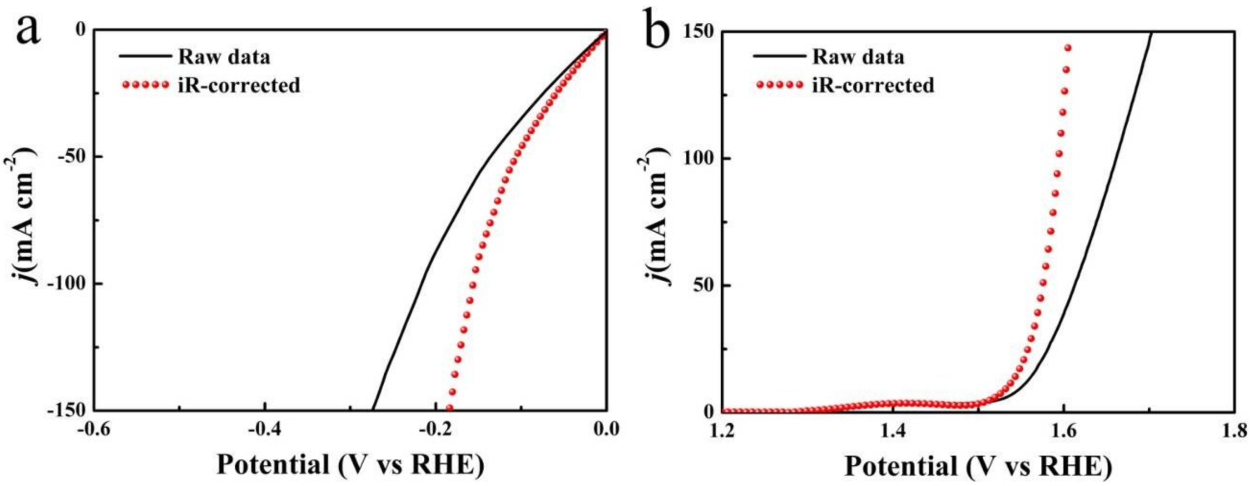

Figure S12. The Polarization curves in 1 M KOH before iR-corrected of $NiSe_2$-$CoSe_2$/NCF. (a) The LSV curves for the HER with a scan rate of 1 mV s^{-1}, and (b) The LSV curves for the OER with a scan rate of 1 mV s^{-1}.

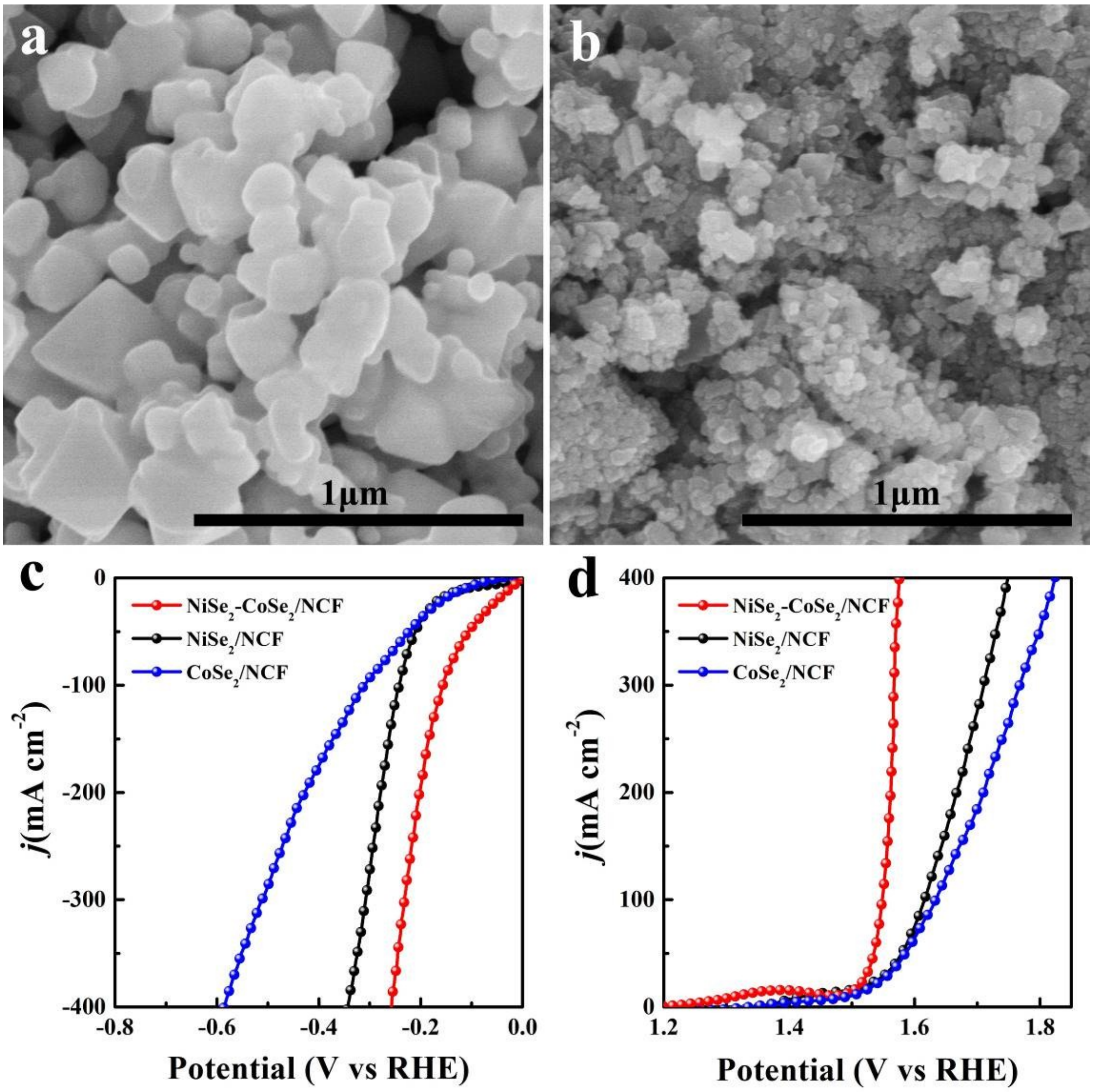

Figure S13. The HER and OER performances of $NiSe_2$/NCF and $CoSe_2$/NCF catalysts.

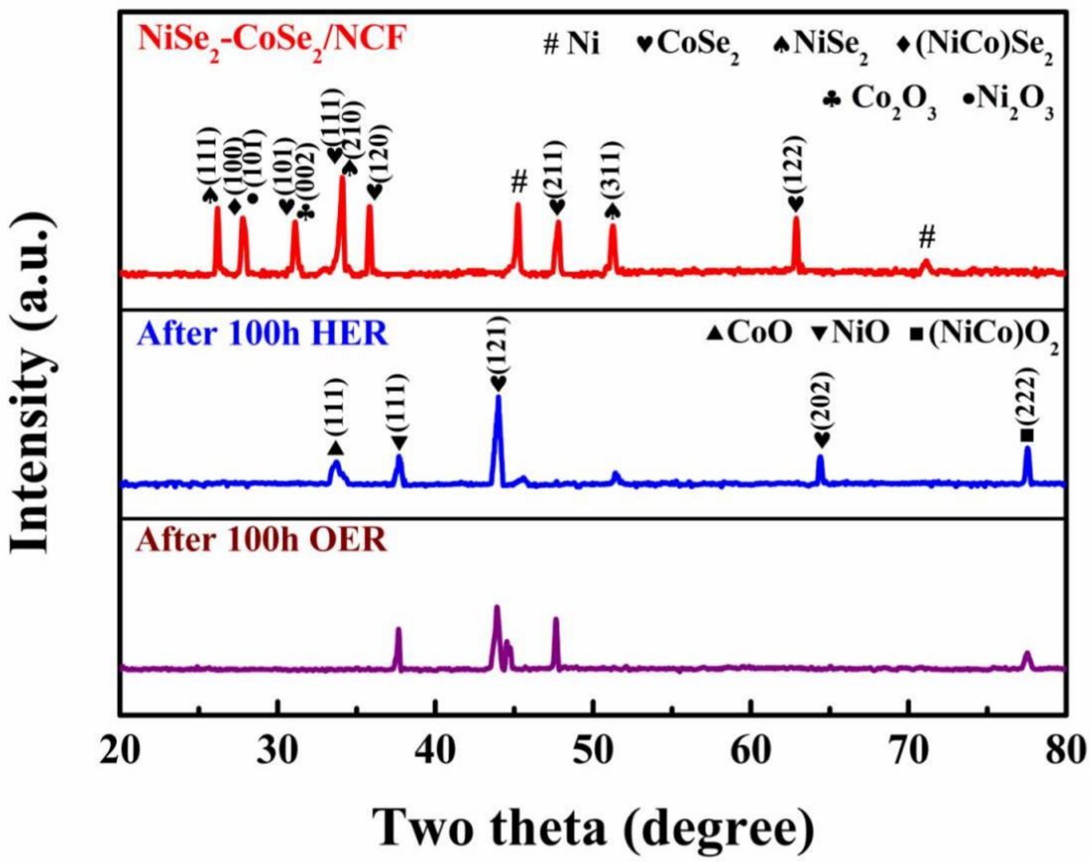

Figure S14. The XRD patterns of the $NiSe_2$-$CoSe_2$/NCF catalysts after the long-term HER and OER processes in 1 M KOH solution at 10 mA cm^{-2} for 100 hours.

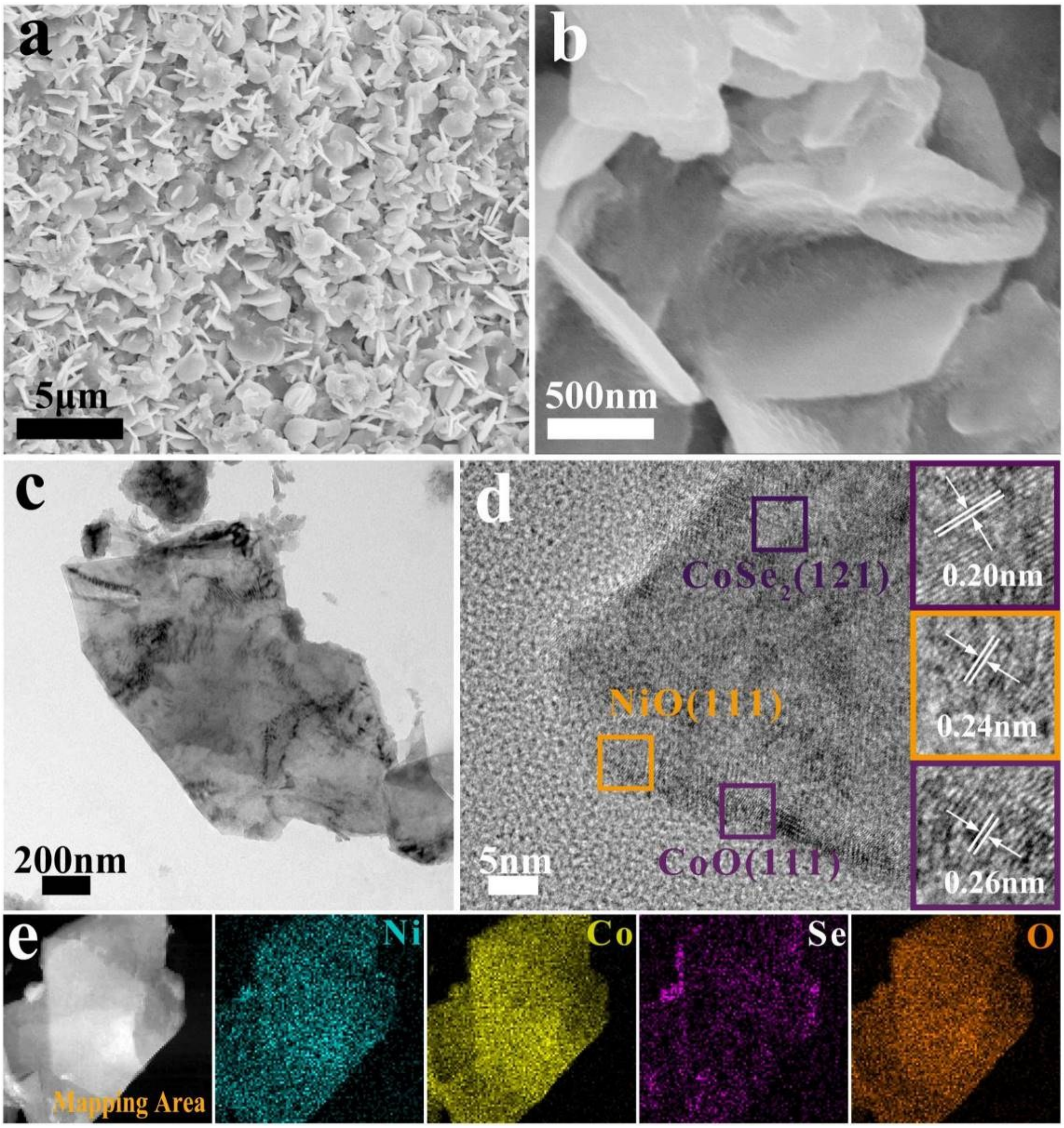

Figure S15. The morphology and crystal structures of $NiSe_2$-$CoSe_2$/NCF samples undergoing a HER process in 1 M KOH solution with j_{10} for 100 h. (a) Low and (b) High resolution SEM, (c) TEM image of $NiSe_2$-$CoSe_2$/NCF nanosheet, (d) High resolution TEM image, and (e) The elements mapping of a single nanosheet.

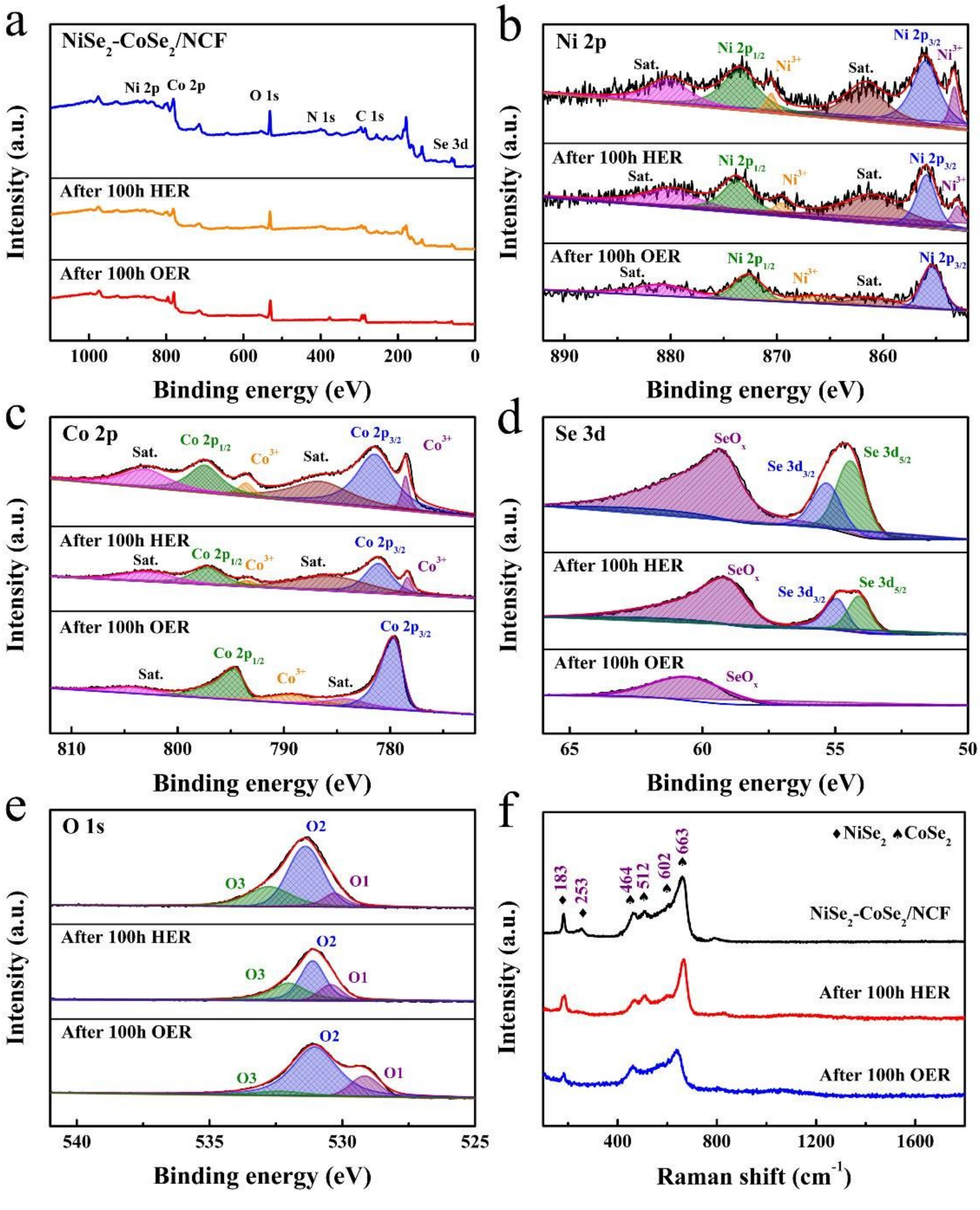

Figure S16. High resolution XPS spectra and the Raman spectra of the $NiSe_2$-$CoSe_2$/NCF undergoing the HER and the OER process in 1 M KOH at j_{10} for 100 h, respectively. (a) The whole spectra, (b) Ni 2p, (c) Co 2p, (d) Se 3d, (e) O 1s, and (f) Raman spectra.

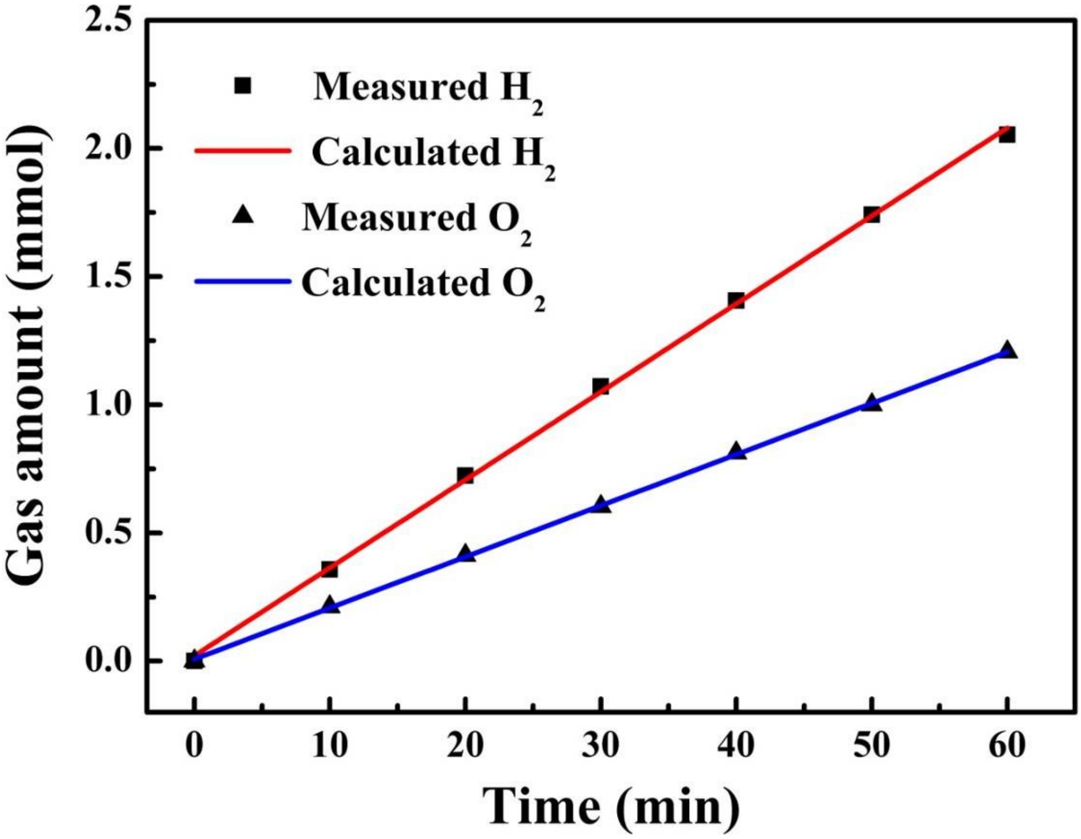

Figure S17. Amounts of gas collected and calculated from the electron quantity of $NiSe_2$-$CoSe_2$/NCF during water splitting, pushing with a current density of j_{10}.

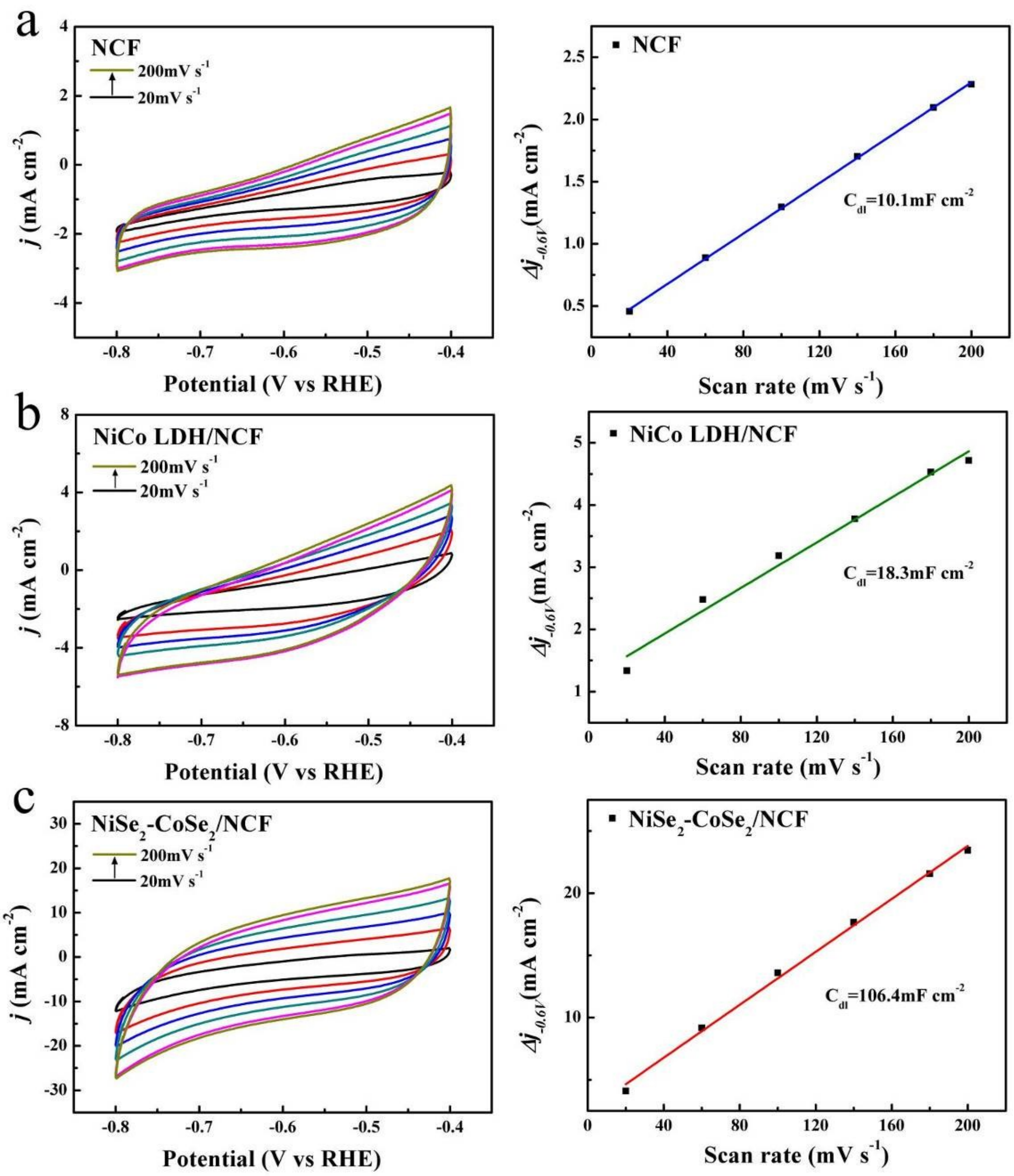

Figure S18. Cyclic voltammograms of the samples at a scan rate from 20 to 200 mV s^{-1} in 1 M KOH (left) and the calculated C_{dl} (right), (a) NCF, (b) NiCo LDH/NCF, and (c) $NiSe_2$-$CoSe_2$/NCF.

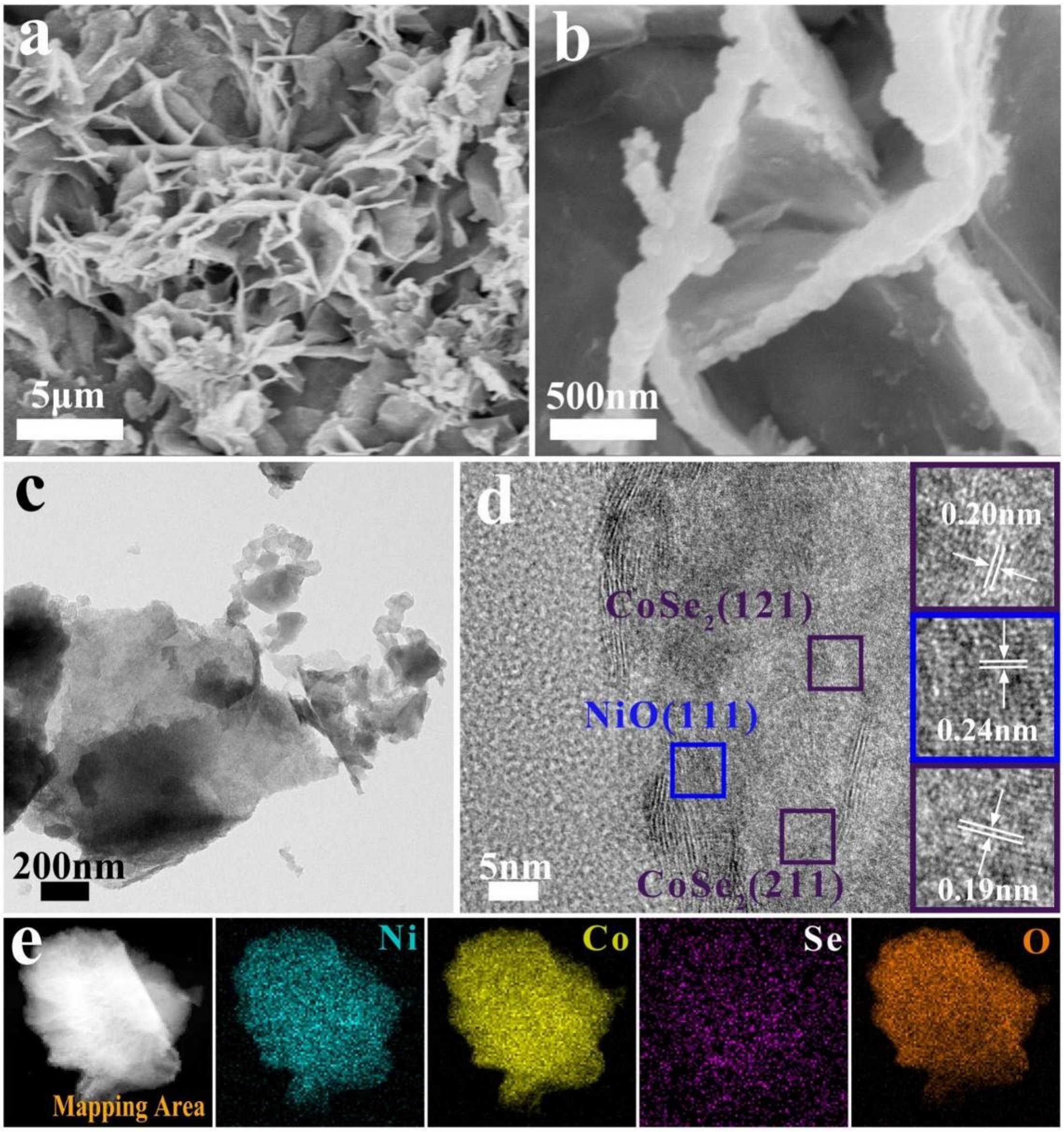

Figure S19. The morphology and crystal planes of $NiSe_2$-$CoSe_2$/NCF undergoing a OER process in 1 M KOH solution at j_{10} for 100 h. (a) Low and (b) High resolution SEM images, (c) Low resolution TEM image, (d) High resolution TEM image, and (e) The elements mapping of a single nanosheet.

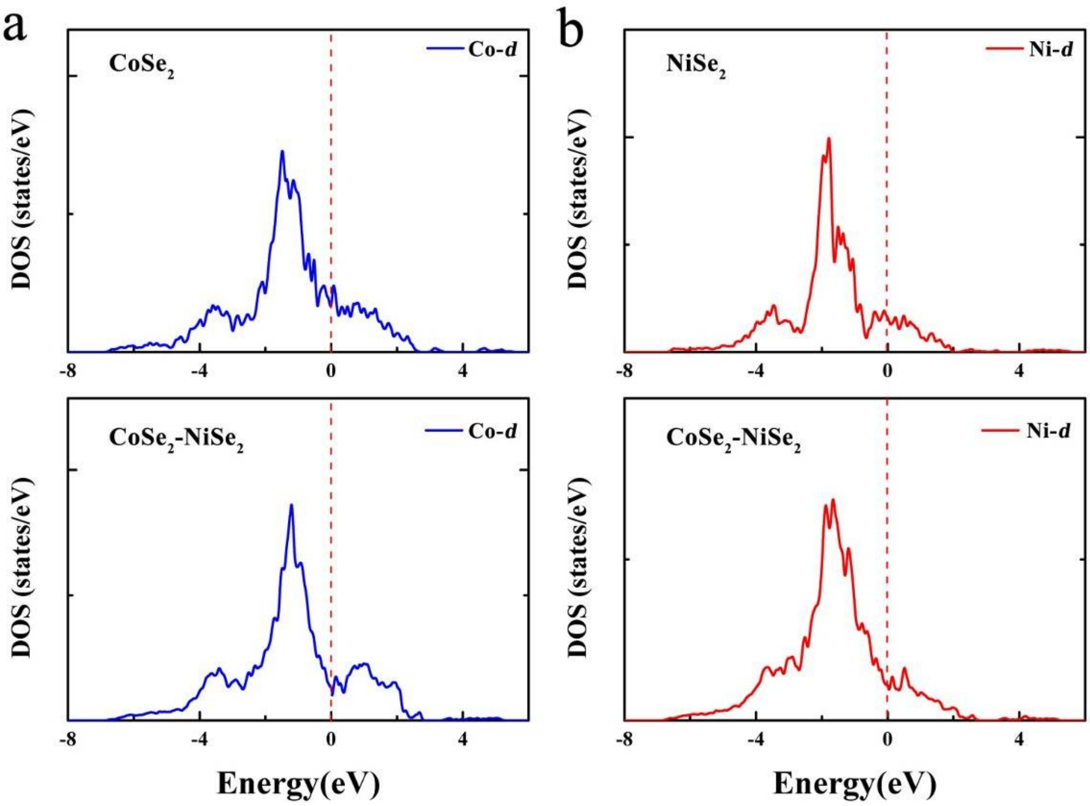

Figure S20. The partial density of state before and after forming the heterojunction. (a) d-band of Co atoms, and (b) d-band of Ni atoms.

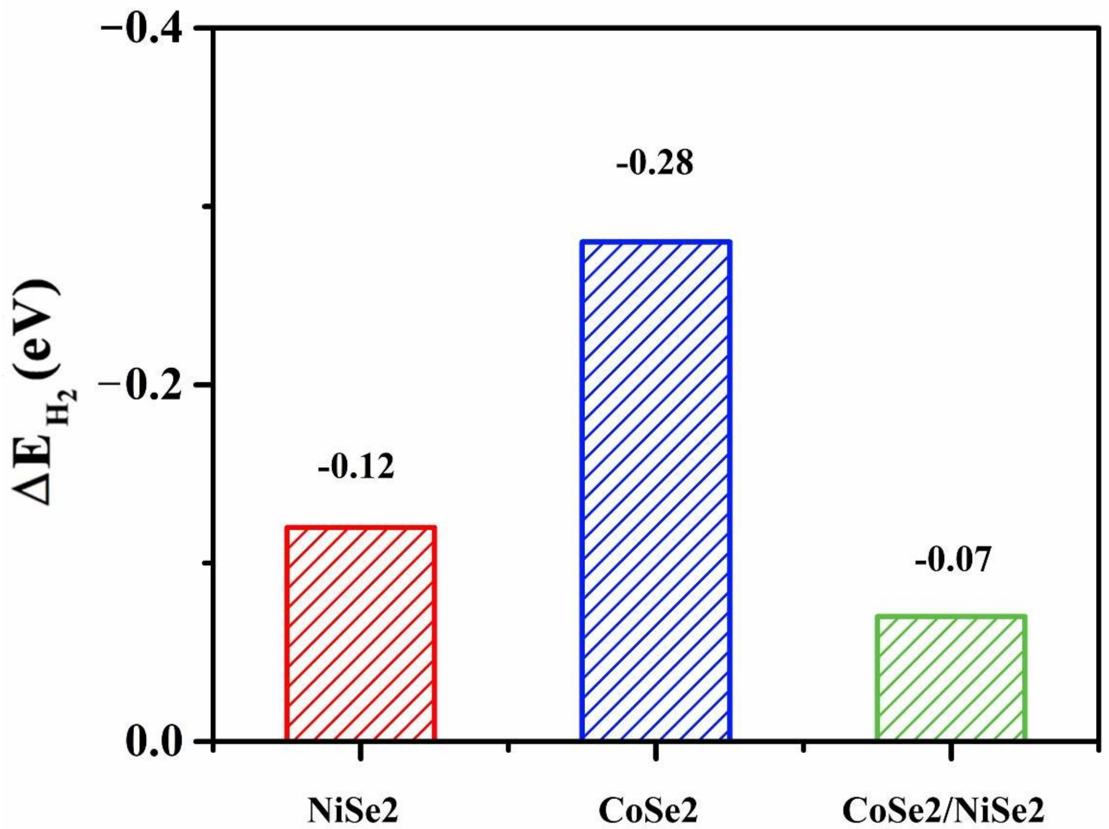

Figure S21. The comparison of the calculated H_2 adsorption energy ($|\Delta E_{H2}|$) for the pure $CoSe_2$, $NiSe_2$ phases and heterointerface-forming $NiSe_2$-$CoSe_2$ phase.

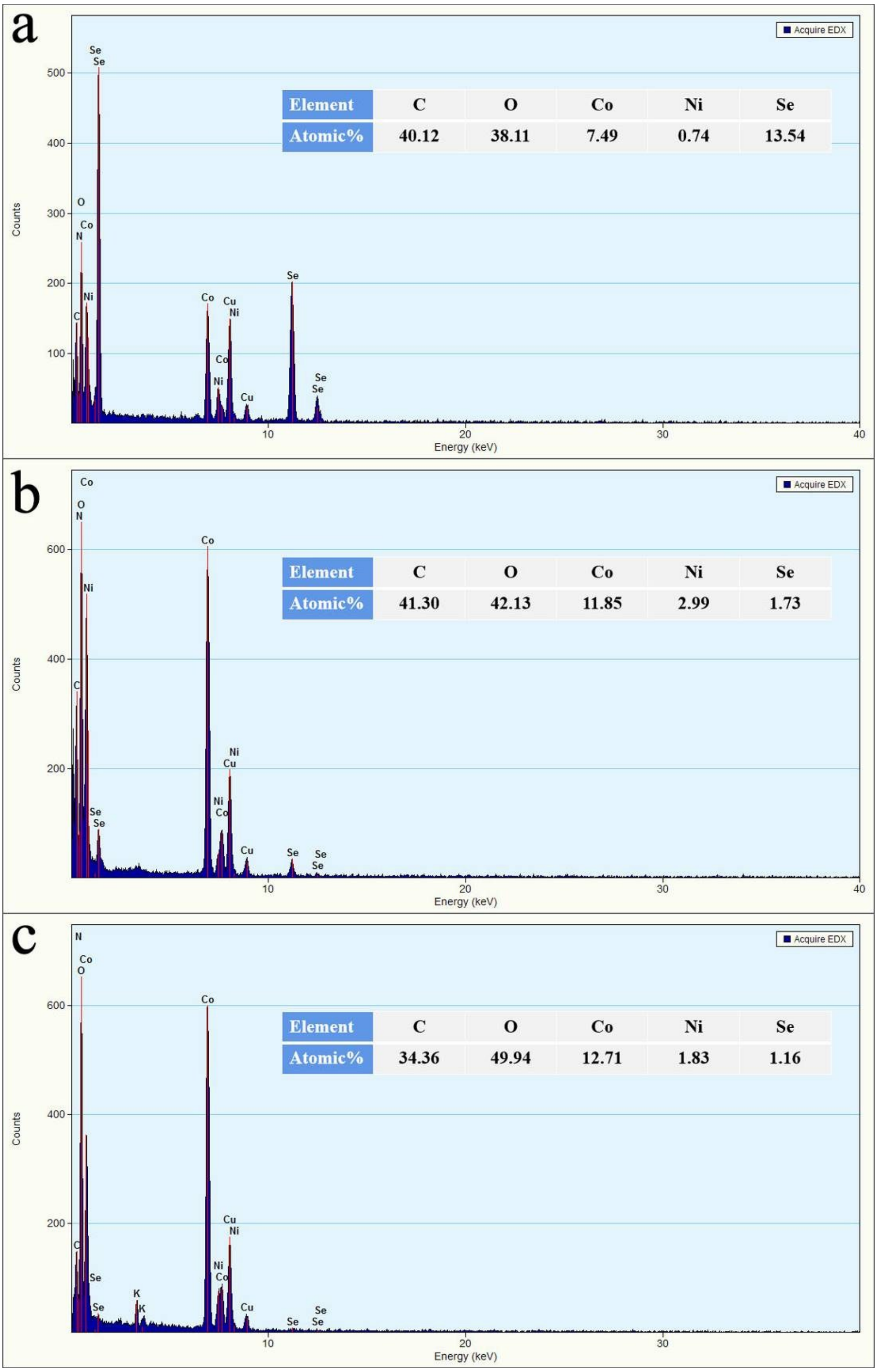

Figure S22. The TEM mode energy-dispersive X-ray (EDX) spectra of $NiSe_2$-$CoSe_2$/NCF catalyst undergoing electrocatalytic processes in 1 M KOH solution with j_{10} for 100 h. (a) The original, (b) After HER, and (c) After OER.

Table S1. The elements contents of different electrocatalysts.

Element / Atomic%	C1s	N1s	O1s	Ni2p	Co2p	Se3d
NCF	54.62	/	33.12	2.64	9.62	/
NiCo LDH/NCF	34.26	/	42.12	6.67	16.95	/
$NiSe_2$-$CoSe_2$/NCF	15.84	9.58	42.04	3.42	17.38	11.74
After 100 h HER	/	3.92	57.32	5.02	21.95	11.79
After 100 h OER	/	/	75.47	2.58	20.27	1.68

Table S2. Elemental composition of the $NiSe_2$-$CoSe_2$/NCF catalyst obtained from ICP-OES.

Element / Atomic%	Ni	Co	Se
$NiSe_2$-$CoSe_2$/NCF	8.04	43.25	48.71

Table S3. The TOF, and Mass Activity (MA) for Pt/C/NCF, NiCo LDH/NCF and $NiSe_2$-$CoSe_2$/NCF corresponding to HER.

Sample	**TOF (s^{-1}@100mV)**	**MA (mA g^{-1}@100mV)**
Pt/C/NCF	2.00×10^{-4}	3.29×10^{3}
NiCo LDH/NCF	5.88×10^{-4}	9.61×10^{2}
$NiSe_2$-$CoSe_2$/NCF	2.13×10^{-3}	1.92×10^{3}

Table S4. TOF for Pt/C/NCF, NiCo LDH/NCF and $NiSe_2$-$CoSe_2$/NCF at an overpotential of 40, 60, 80, 100 and 200 mV corresponding to HER.

TOF s^{-1}	**Pt/C/NCF**	**NiCo LDH/NCF**	**$NiSe_2$-$CoSe_2$/NCF**
40 mV	2.35×10^{-5}	7.40×10^{-5}	7.61×10^{-4}
60 mV	5.68×10^{-5}	1.79×10^{-4}	1.18×10^{-3}
80 mV	1.19×10^{-4}	3.49×10^{-4}	1.64×10^{-3}
100 mV	2.00×10^{-4}	5.88×10^{-4}	2.13×10^{-3}
200 mV	6.54×10^{-4}	6.76×10^{-3}	9.00×10^{-3}

Table S5. Comparison of electrocatalytic HER activity of various non-precious catalysts in 1.0 M KOH electrolyte.

Catalysts	**η (mV) @ *J* (mA cm^{-2})**	**Tafel slope**	**Stability (h) @ *J* (mA cm^{-2})**	**References**
$NiSe_2$-$CoSe_2$/NCF	24@10 106@50 156@100 202@200 231@300 257@400	24 mV dec^{-1}	100@10 100@100	This Work
NiFe LDH@NiCoP/NF	120@10 320@100	89 mV dec^{-1}	100@10	[S1]
Se-(NiCo)S/OH	103@10 204@100	88 mV dec^{-1}	80@10	[S2]
$Fe_{0.09}Co_{0.13}$-$NiSe_2$/CFC	92@10 215@100 251@200	89 mV dec^{-1}	50@10	[S3]
$(Ni,Co)_{0.85}Se$ NSAs	169@10 284@100 317@200	116 mV dec^{-1}	12@25	[S4]
NiFeSe@NiSe|O@CC	62@10 231@100 342@200	49 mV dec^{-1}	50@10	[S5]
Co-B/Ni	70@10 345@200 408@400	68 mV dec^{-1}	20@50	[S6]
Ni-Co-P HNBs	107@10 209@200	46 mV dec^{-1}	20@100	[S7]
$Fe_{7.4\%}$-NiSe	163@10 283@300	72 mV dec^{-1}	22@20	[S8]
W- NiCoP/NF	30@10 170@200 211@400	35 mV dec^{-1}	24@10	[S9]
NiCoP@NC NA/NF	37@10 123@50 205@100	54 mV dec^{-1}	22@10	[S10]

CoP-Co_2P@PC/PG NHs	39@10 68@50	59 mV dec^{-1}	30@10	[S11]
$WS_{2(1-x)}Se_{2x}/NiSe_2$	88@10 129@50 146@100	47 mV dec^{-1}	10@120	[S12]
***o*-$CoSe_2$|P**	104@10 177@100 193@200 205@300	69 mV dec^{-1}	20@100	[S13]
N-NiCoP/NF	78@10 180@50 211@100	83 mV dec^{-1}	100@10	[S14]
NiCoP/NF	32@10	37 mV dec^{-1}	24@10	[S15]
$NiCo_2O_4$	110@10 245@100	50 mV dec^{-1}	32@10	[S16]
Co_1Mn_1CH	180@10 281@50 328@100	N/A	10@10	[S17]

Table S6. The TOF, and Mass Activity (MA) for RuO_2/NCF, NiCo LDH/NCF and $NiSe_2$-$CoSe_2$/NCF corresponding to OER.

Sample	TOF (s^{-1}@300mV)	MA (mA g^{-1}@300mV)
RuO_2/NCF	9.66×10^{-2}	8.14×10^{2}
NiCo LDH/NCF	1.15×10^{-1}	4.61×10^{2}
$NiSe_2$-$CoSe_2$/NCF	4.55×10^{-1}	5.28×10^{2}

Table S7. TOF for RuO_2/NCF, NiCo LDH/NCF and $NiSe_2$-$CoSe_2$/NCF at an overpotential of 250, 275, 300, and 325 mV corresponding to OER.

TOF s^{-1}	**RuO_2/NCF**	**NiCo LDH/NCF**	**$NiSe_2$-$CoSe_2$/NCF**
250 mV	4.45×10^{-2}	1.11×10^{-1}	1.20×10^{-1}
275 mV	6.93×10^{-2}	1.05×10^{-1}	1.77×10^{-1}
300 mV	9.66×10^{-2}	1.15×10^{-1}	4.55×10^{-1}
325 mV	1.32×10^{-1}	1.77×10^{-1}	1.60

Table S8. Comparison of electrocatalytic OER activity of various non-precious catalysts in 1.0 M KOH electrolyte.

Catalysts	***η* (mV) @ *J* (mA cm^{-2})**	**Tafel slope**	**Stability (h) @ *J* (mA cm^{-2})**	**References**
$NiSe_2$-$CoSe_2$/NCF	250@10 305@50 318@100 332@200 337@300 346@400	48 mV dec^{-1}	100@10 100@100	This Work
NiFe LDH@NiCoP/NF	220@10 345@100 459@200 560@300	49 mV dec^{-1}	100@10	[S1]
Se-(NiCo)S/OH	155@10 242@100 296@200	34 mV dec^{-1}	73@20	[S2]
$(Ni,Co)_{0.85}Se$ NSAs	287@20 398@200 470@400	87 mV dec^{-1}	12@72	[S4]
Co-B/Ni	140@10 412@100 524@200	98 mV dec^{-1}	20@100	[S6]
$Fe_{7.4\%}$-NiSe	231@50 257@300	43 mV dec^{-1}	22@30	[S8]
N-NiCoP/NF	225@10 361@100	67 mV dec^{-1}	100@10	[S14]
NiCoP/NF	280@10 300@16	87 mV dec^{-1}	24@10	[S15]
$NiCo_2O_4$	290@10 330@50 360@100	53 mV dec^{-1}	32@10	[S16]
Co_1Mn_1CH	322@50 349@100	N/A	18@50	[S17]
NiCo-nitrides/$NiCo_2O_4$/GF	183@10 435@100 538@200	56 mV dec^{-1}	40@10	[S18]

Ni_5Co_3Mo-OH	280@50 290@100 301@200 320@300	57 mV dec^{-1}	100@100	[S19]
$Ni_{0.33}Co_{0.67}MoS_4$/CFC	283@10 344@100	69 mV dec^{-1}	10@10	[S20]
FeOOH(Se)/IF	287@10 363@100 405@200 449@400	54 mV dec^{-1}	15@10	[S21]
LSC&$MoSe_2$	370@10 487@100	77 mV dec^{-1}	1000@100	[S22]
$CoSe_{1.26}P_{1.42}$	255@10 333@50 372@100	87 mV dec^{-1}	15@10	[S23]
5% Fe-$NiSe_2$	231@10 368@100 241@200	83 mV dec^{-1}	20@15	[S24]
two-tiered NiSe	290@10 354@50 421@100	77 mV dec^{-1}	30@10	[S25]

Table S9. Comparison of overall water splitting performance of this work with recently reported electrocatalysts in 1 M KOH solution at the current density of 50, 100 and 200 mA cm^{-2}.

Catalysts	Cell voltages (V) @ *J* (mA cm^{-2})	References
$NiSe_2$-$CoSe_2$/NCF	1.63@50 1.69@100 1.79@200	This work
NiFe LDH@NiCoP/NF	1.76@50 1.91@100	[S1]
Se-(NiCo)S/OH	1.86@50 2.04@100	[S2]
$(Ni,Co)_{0.85}Se$ NSAs	1.88@50 1.98@80	[S4]
NiFeSe@NiSe|O@CC	1.72@50 1.86@100	[S5]
$Fe_{7.4\%}$-NiSe	1.68@50 1.73@100	[S8]
N-NiCoP/NF	1.56@10 1.82@100	[S14]
NiCoP/NF	1.65@50 1.81@100	[S15]
$NiCo_2O_4$	1.65@10	[S16]
Co_1Mn_1CH	1.83@50 1.98@100	[S17]
Co-Ni-Se/C/NF	1.76@50 1.87@100	[S26]
Co-B@CoO	1.67@50	[S27]
FeCoNi-LTH/$NiCo_2O_4$/CC	1.65@50	[S28]
Ru-HPC||P-RuO_2	1.64@50 1.69@100	[S29]
$NiCo_2S_4$-2	1.80@50 1.96@100	[S30]

References

(S1) H. Zhang, X. Li, A. Hähnel, V. Naumann, C. Lin, S. Azimi, S. L. Schweizer, A. W. Maijenburg, R. B. Wehrspohn, Bifunctional heterostructure assembly of NiFe LDH nanosheets on NiCoP nanowires for highly efficient and stable overall water splitting, *Advanced Functional Materials* **2018**, *28*, 1706847.

(S2) C. Hu, L. Zhang, Z. J. Zhao, A. Li, X. Chang, J. Gong, Synergism of geometric construction and electronic regulation: 3D Se-$(NiCo)S_x/(OH)_x$ nanosheets for highly efficient overall water splitting, *Adv. Mater.* **2018**, *30*, 1705538.

(S3) Y. Sun, K. Xu, Z. Wei, H. Li, T. Zhang, X. Li, W. Cai, J. Ma, H. J. Fan, Y. Li, Strong electronic interaction in dual-cation-incorporated $NiSe_2$ nanosheets with lattice distortion for highly efficient overall water splitting, *Adv. Mater.* **2018**, *30*, 1802121.

(S4) K. Xiao, L. Zhou, M. Shao, M. Wei, Fabrication of $(Ni,Co)_{0.85}Se$ nanosheet arrays derived from layered double hydroxides toward largely enhanced overall water splitting, *Journal of Materials Chemistry A* **2018**, *6*, 7585-7591.

(S5) G. Yilmaz, C. F. Tan, Y. F. Lim, G. W. Ho, Pseudomorphic transformation of interpenetrated prussian blue analogs into defective nickel iron selenides for enhanced electrochemical and photo-electrochemical water splitting, *Advanced Energy Materials* **2019**, *9*, 1802983.

(S6) W. Hao, R. Wu, R. Zhang, Y. Ha, Z. Chen, L. Wang, Y. Yang, X. Ma, D. Sun, F. Fang, Y. Guo, Electroless plating of highly efficient bifunctional boride-based electrodes toward practical overall water splitting, *Advanced Energy Materials* **2018**, *8*, 1801372.

(S7) E. Hu, Y. Feng, J. Nai, D. Zhao, Y. Hu, X. W. D. Lou, Construction of hierarchical Ni-Co-P hollow nanobricks with oriented nanosheets for efficient overall water splitting, *Energy & Environmental Science* **2018**, *11*, 872-880.

(S8) Z. Zou, X. Wang, J. Huang, Z. Wu, F. Gao, An Fe-doped nickel selenide nanorod/nanosheet hierarchical array for efficient overall water splitting, *Journal of Materials Chemistry A* **2019**, *7*, 2233-2241.

(S9) S. Lu, L. Zhang, Y. Dong, J. Zhang, X. Yan, D. Sun, X. Shang, J. Chi, Y. Chai, B. Dong, Tungsten-doped Ni-Co phosphides with multiple catalytic sites as efficient electrocatalysts for overall water splitting, *Journal of Materials Chemistry A* **2019**, *7*, 16859-16866.

(S10) B. Cao, Y. Cheng, M. Hu, P. Jing, Z. Ma, B. Liu, R. Gao, J. Zhang, Efficient and durable 3D self-supported nitrogen-doped carbon-coupled nickel/cobalt phosphide electrodes: stoichiometric ratio regulated phase- and morphology dependent overall water splitting performance, *Advanced Functional Materials* **2019**, *29*, 1906316.

(S11) J. Yang, D. Guo, S. Zhao, Y. Lin, R. Yang, D. Xu, N. Shi, X. Zhang, L. Lu, Y. Q. Lan, J. Bao, M. Han, Cobalt phosphides nanocrystals encapsulated by p-doped carbon and married with p-doped graphene for overall water splitting, *Small* **2019**, *15*, 1804546.

(S12) H. Zhou, F. Yu, J. Sun, H. Zhu, I. K. Mishra, S. Chen, Z. Ren, Highly efficient hydrogen evolution from edge-oriented $WS_{2(1-x)}Se_{2x}$ particles on three-dimensional porous $NiSe_2$ foam, *Nano Lett* **2016**, *16*, 7604 -7609.

(S13) Y. R. Zheng, P. Wu, M. R. Gao, X. L. Zhang, F. Y. Gao, H. X. Ju, R. Wu, Q. Gao, R. You, W. X. Huang, S. J. Liu, S. W. Hu, J. Zhu, Z. Li, S. H. Yu, Doping-induced structural phase transition in cobalt diselenide enables enhanced hydrogen evolution catalysis, *Nature communications* **2018**, *9*, 2533.

(S14) R. Zhang, J. Huang, G. Chen, W. Chen, C. Song, C. Li, K. Ostrikov, In situ engineering bi-metallic phospho-nitride bi-functional electrocatalysts for overall water splitting, *Applied Catalysis B: Environmental* **2019**, *254*, 414-423.

(S15) H. F. Liang, A. N. Gandi, D. H. Anjum, X. B. Wang, U. Schwingenschlögl, H. S. N. Alshareef, Plasma-Assisted Synthesis of NiCoP for Efficient Overall Water Splitting, *Nano Lett* **2016**, *16*, 7718-7725.

(S16) X. H. Gao, H. X. Zhang, Q. G. Li, X. G. Yu, Z. L. Hong, X. W. Zhang, C. D. Liang, Z. Lin, Hierarchical $NiCo_2O_4$ Hollow Microcuboids as Bifunctional Electrocatalysts for Overall Water-Splitting, *Angew. Chem. Int. Ed* **2016**, *55*, 6290-6294.

(S17) T. Tang, W. J. Jiang, S. Niu, N. Liu, H. Luo, Y. Y. Chen, S. F. Jin, F. Gao, L. J. Wan, J. S. Hu, Electronic and Morphological Dual Modulation of Cobalt Carbonate Hydroxides by Mn Doping toward Highly Efficient and Stable Bifunctional Electrocatalysts for Overall Water Splitting, *J. Am. Chem. Soc* **2017**, *139*, 8320-8328.

(S18) Z. Liu, H. Tan, D. Liu, X. Liu, J. Xin, J. Xie, M. Zhao, L. Song, L. Dai, H. Liu, Promotion of overall water splitting activity over a wide pH range by interfacial electrical effects of metallic NiCo-nitrides nanoparticle/$NiCo_2O_4$ nanoflake/graphite fibers, *Advanced Science* **2019**, *6*, 1801829.

(S19) S. Hao, L. Chen, C. Yu, B. Yang, Z. Li, Y. Hou, L. Lei, X. Zhang, NiCoMo hydroxide nanosheet arrays synthesized via chloride corrosion for overall water splitting, *ACS Energy Letters* **2019**, *4*, 952-959.

(S20) L. Hang, T. Zhang, Y. Sun, D. Men, X. Lyu, Q. Zhang, W. Cai, Y. Li, $Ni_{0.33}Co_{0.67}MoS_4$ nanosheets as a bifunctional electrolytic water catalyst for overall water splitting, *Journal of Materials Chemistry A* **2018**, *6*, 19555-19562.

(S21) S. Niu, W. J. Jiang, Z. Wei, T. Tang, J. Ma, J. S. Hu, L. J. Wan, Se-doping activates FeOOH for cost-effective and efficient electrochemical water oxidation, *Journal of the American Chemical Society* **2019**, *141*, 7005-7013.

(S22) N. K. Oh, C. Kim, J. Lee, O. Kwon, Y. Choi, G. Y. Jung, H. Y. Lim, S. K. Kwak, G. Kim, H. Park, In-situ local phase-transitioned $MoSe_2$ in $La_{0.5}Sr_{0.5}CoO_{3-\delta}$ heterostructure and stable overall water electrolysis over 1000 hours, *Nature communications* **2019**, *10*, 1723.

(S23) Y. Zhu, H. C. Chen, C. S. Hsu, T. S. Lin, C. J. Chang, S. C. Chang, L. D. Tsai, H. M. Chen, Operando unraveling the structural/chemical stability of P substituted $CoSe_2$ electrocatalysts toward hydrogen/oxygen evolution reactions in alkaline electrolyte, *ACS Energy Letters* **2019**, *4*, 987-994.

(S24) L. Lin, M. Chen, L. Wu, Hierarchical iron-doped nickel diselenide hollow spheres for efficient oxygen evolution electrocatalysis, *ACS Applied Energy Materials* **2019**, *2*, 4737-4744.

(S25) H. Wu, X. Lu, G. Zheng, G. W. Ho, Topotactic engineering of ultrathin 2D nonlayered nickel selenides for full water electrolysis, *Advanced Energy Materials* **2018**, *8*, 1702704.

(S26) F. Ming, H. Liang, H. Shi, X. Xu, G. Mei, Z. Wang, MOF-derived Co-doped nickel selenide/C electrocatalysts supported on Ni foam for overall water splitting, *Journal of Materials Chemistry A* **2016**, *4*, 15148-15155.

(S27) W. Lu, T. Liu, L. Xie, C. Tang, D. Liu, S. Hao, F. Qu, G. Du, Y. Ma, A. M. Asiri, In situ derived Co-B nanoarray: a high-efficiency and durable 3D bifunctional electrocatalyst for overall alkaline water splitting, *Small* **2017**, *13*, 1700805.

(S28) Y. Liu, Y. Bai, Y. Han, Z. Yu, S. Zhang, G. Wang, J. Wei, Q. Wu, K. Sun, Self-supported hierarchical FeCoNi-LTH/$NiCo_2O_4$/CC electrodes with enhanced bifunctional performance for efficient overall water splitting, *ACS Applied Materials & Interfaces* **2017**, *9*, 36917-36926.

(S29) T. Qiu, Z. Liang, W. Guo, S. Gao, C. Qu, H. Tabassum, H. Zhang, B. Zhu, R. Zou, Y. Shao-Horn, Highly exposed ruthenium-based electrocatalysts from bimetallic metal-organic frameworks for overall water splitting, *Nano Energy* **2019**, *58*, 1-10.

(S30) Z. Kang, H. Guo, J. Wu, X. Sun, Z. Zhang, Q. Liao, S. Zhang, H. Si, P. Wu, L. Wang, Y. Zhang, Engineering an earth-abundant element-based bifunctional electrocatalyst for highly efficient and durable overall water splitting, *Advanced Functional Materials* **2019**, *29*, 1807031.